ACS SENSORS

pubs.acs.org/acssensors

Article

High-Sensitivity Micro-Gas Chromatograph–Photoionization Detector for Trace Vapor Detection

Maxwell Wei-Hao Li,[‖] Abhishek Ghosh,[‖] Anandram Venkatasubramanian, Ruchi Sharma, Xiaolu Huang, and Xudong Fan*

Cite This: *ACS Sens.* 2021, 6, 2348–2355

Read Online

ACCESS | Metrics & More | Article Recommendations | Supporting Information

ABSTRACT: Rapid *in situ* detection and analysis of trace vapor concentrations at a sub-parts per billion to parts per trillion level remains a challenge for many applications such as indoor air-quality analysis and detection of explosives and narcotics. Micro-gas chromatography (μGC) together with a micro-photoionization detector (μPID) is a prominent method for portable analysis of complex vapor mixtures, but current μPID technology demonstrates poor detection performance compared to benchtop flame ionization detectors (FIDs). This work demonstrates the development of a significantly improved μPID with a sub-picogram detection limit (as low as ~0.2 pg) comparable to or exceeding that of a benchtop FID, with a large linear dynamic range (>4 orders of magnitude) and robustness (high stability over 200 h of plasma activation). Based on this μPID, a complete μGC–PID system was built and tested on standard sample chromatograms in a laboratory setting to show the system's analytical capabilities and the detection limit down to sub-parts per trillion concentrations (as low as 0.14 ppt). Practical in-field chromatograms on breath and car exhaust were also generated to demonstrate applicability for *in situ* experimentation. This work shows that μGC–PID systems can be competitive with traditional GC–FID methods and thus opens a door to rapid trace vapor analysis in the field.

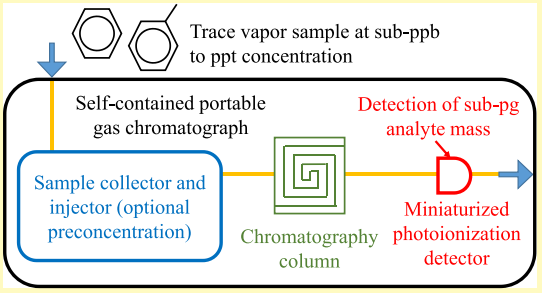

KEYWORDS: *photoionization detector, volatile organic compounds, portable gas chromatography, trace vapor analysis, low detection limit, high sensitivity*

INTRODUCTION

Micro-gas chromatography (μGC) devices have recently been of increasing importance for rapid *in situ* analysis of volatile organic compounds (VOCs) and target a broad range of applications such as environmental monitoring, gas leak detection, and healthcare. A particular point of interest is sensing of trace VOCs for applications such as indoor air screening or detection of explosives and narcotics, which critically require highly sensitive vapor detectors which ultimately determine the sensitivity of μGC systems. Over the past few decades, a variety of miniaturized vapor detectors have been developed that can be used in μGC, including miniaturized thermal conductivity detectors, surface acoustic wave detectors, chemiresistors, chemicapacitors, and electron capture detectors.[1−15] In general, although these micro-detectors can achieve extremely small footprint and low operating costs (power and gas consumption), their sensitivity is typically poor compared to the flame ionization detectors (FIDs) widely used in benchtop GC systems, which μGC systems aim to supplement or replace. While FIDs may possess detection limits on the order of sub-picogram or sub-parts per trillion concentrations (e.g., considering a mass of ~1 pg in 1 L volume), most miniaturized detectors have detection limits around a few parts per million or at best tens of parts per billion.[1−13] This poor performance presents a problem for the aforementioned trace vapor analysis applications, which require near picogram detection limits, corresponding to parts per trillion to sub-parts per billion concentration levels (~ng/L or sub ng/L). Table S1 provides an example list of target detection or screening levels set by the EPA for the investigation of regional screening of carcinogens.

Another miniaturized vapor detector suitable for μGC is the micro-photoionization detector (μPID),[16−46] which uses noble or permanent gases (e.g., xenon, krypton, argon, and helium) to excite plasma and generate photons ranging from 9.6 to 17.5 eV. μPIDs have been shown to possess reasonable detection limits (down to tens of picograms) and dynamic ranges (up to 6 decades), and miniaturization efforts have allowed for lower manufacturing costs, faster response times, and smaller footprints.[17,19,20,25,28−35,42,44−46] In particular, Zhu et al. reported a microfabricated μPID device demonstrating

Received: March 5, 2021
Accepted: May 10, 2021
Published: May 24, 2021

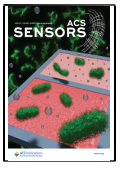

https://doi.org/10.1021/acssensors.1c00482
ACS Sens. 2021, 6, 2348–2355

single-digit picogram detection limits, tens of milliseconds response time, and low operating voltage (6 VDC).[25] Despite these advances, the detection limit of these μPID devices is still comparatively higher than that of benchtop FIDs, presenting some limitations for low-concentration chemical analysis. Further improvement of performance, especially the detection limit, is required for μPIDs and μGC−PID systems to be competitive with the current conventional benchtop GC−FID method.

This paper details the development of a highly sensitive chip-based μPID with a sub-picogram detection limit and a wide linear dynamic range. In particular, side-by-side comparison shows that the detection limit of the μPID is 2−4 times better than a commercial Agilent FID over a broad range of VOCs. Based on this μPID, a complete, automated, highly robust μGC−PID system was constructed using in-house fabricated microcomponents, including a miniaturized preconcentrator, microcolumn (μcolumn), and μPID, as well as in-house-developed PID circuits. The whole system is self-contained within a box of dimensions 27 × 24 × 10 cm and can be independently operated without the use of any benchtop equipment (besides a laptop for readout). Due to the highly sensitive μPID, this system is capable of detecting sub-parts per trillion concentrations of VOCs with a 200 mL sample volume, which was enabled by the miniaturized preconcentrator. This paper details the μPID fabrication procedure and characterization along with system-level assembly, with emphasis on μPID and μGC−PID performance for detection of trace VOCs. Both standard sample chromatograms and practical chromatograms are also provided, exhibiting the capability of the μGC−PID to match or even surpass the benchtop GC−FID detection limit. This would enable use of this μGC−PID system to supplement or replace the need for conventional benchtop GC analysis for on-site low concentration VOC analysis.

EXPERIMENTAL SECTION

Materials. Analytical standard-grade hexane, heptane, octane, nonane, decane, undecane, benzene, toluene, ethylbenzene, o-xylene, chlorobenzene, ethyl acetate, butyl acetate, acetone, methyl isobutyl ketone, 2-pentanone, 2-hexanone, 2-heptanone, tetrahydrofuran, 2-butanol, isopropanol, hexamethyldisilazane (HMDS), and EPA 502/524.4 VOC mix were purchased from Sigma-Aldrich (St. Louis, MO). N-type silicon wafers (P/N 1095, 100 mm diameter, 500 μm thickness) and Borofloat 33 glass (P/N 517) were purchased from University Wafer. Carbopack B (P/N 20273) and X (P/N 10437-U) were purchased from Sigma-Aldrich. Additional accessory materials are provided in Table S2. All materials were used as purchased without further purification or modification. 99.5% purity helium (P/N 49615He) was used as the carrier gas and was purchased from Leland Gas Technologies (South Plainfield, NJ).

Component Fabrication. The μPID chip was fabricated according to the fabrication process and pattern shown in Figure S1, which were adapted from our previous work.[25] The pattern was modified to form a circular spiral with a wider channel width of 400 μm. This allowed for a larger illumination area of ∼14 mm^2 from 3.5 mm^2 in the previous design in ref 25 and increased flow rates through the channel. After dicing, the chip was immersed in acetone and baked out at 80 °C for 1 h. A photograph of the μPID chip is also provided in Figure S1. Subsequently, a VUV krypton lamp was then mounted atop the microchannel and sealed with Norland optical adhesive, with fluidic connections simultaneously formed by inserting guard columns into the inlet and outlet and sealing with the same optical adhesive. Prior to electrode formation, the silicon contact resistance was reduced to 10 kΩ, critically improving μPID's sensitivity. Readout electrodes were then formed by depositing MG Chemicals silver conductive epoxy and attaching wires. An in-house-developed circuit shown in Figure S2 was used for μPID plasma generation and readout. The bias voltage was notably increased to 24 V to from 6 V (in ref 25) to accommodate the wider channel width.

5 and 10 m μcolumns were fabricated according to the fabrication process in Figure S3. The columns were deactivated by eight repeated injections of HMDS at 120 °C over 2 h. The columns were both dynamically coated with a 3% (w/w) solution of OV-1 in dichloromethane by injecting 1 mL of solution and pushing out at a rate of 5 cm/min. The columns were subsequently treated with HMDS again (eight injections at 120 °C over 2 h) and then baked out at 220 °C for 2 h prior to use. The resistance of the integrated heater was measured to be 22 Ω for the 5 m column and 28 Ω for the 10 m column and wire bonded to a PCB board to allow for pulse-width-modulated heating using a peak voltage of 24 V. The maximum temperature ramping rate was estimated to be around 10 °C/s (up to 150 °C), although typical temperature ramping rates used ranged from around 30 to 60 °C/min.

The stainless-steel preconcentrator was made by first cutting a 21.5 gauge stainless-steel tube to 4.5 cm in length. One end was first plugged with glass wool. Subsequently, the tube was filled with 0.75 mg of Carbopack B, followed by 0.75 mg of Carbopack X, and the other end was then plugged with glass wool again. Two universal press-tight connectors were attached to both ends of the stainless-steel tube after loading and fixed using Hysol epoxy. A very thin layer of epoxy (∼0.2 mm) was also applied to the outer surface of the stainless-steel tube body. The entire preconcentrator was placed into an oven at 120 °C and left to dry for 12 h. Finally, 32 gauge nickel chromium wire (resistance ∼7 Ω) was wrapped around the stainless steel tube body for heating.

System Setup and Experimental Conditions. The μGC−PID system was assembled by forming fluidic connections using universal press-tight connectors and deactivated fused silica capillaries between the injector, μcolumn, and μPID. Both the plasma excitation voltage and baseline voltage trimming were carefully tuned to improve the signal-to-noise-ratio (SNR) of the system. Furthermore, relevant electronic components (especially the μPID) were shielded with copper mesh to further reduce the noise. A fluidic diagram is provided in Figure 1, and a picture of the system is provided in Figure 2. The

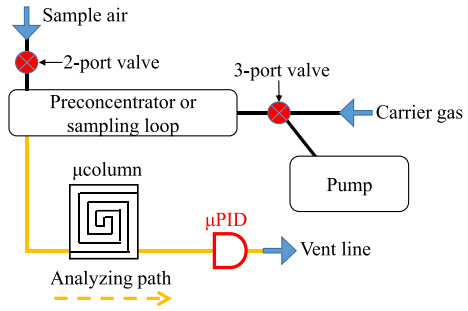

Figure 1. μGC−PID system fluidic diagram. The system is entirely self-contained, excluding the computer at signal output. Either a sampling loop or preconcentrator can be used for sample injection. The μcolumn was coated with a 3% (w/w) solution of OV-1. A picture of the μPID system is provided in Figure 2.

whole system is self-contained within a box of dimensions 27 × 24 × 10 cm (excluding a laptop for readout). The system was evaluated using either a 12 cm (1.875 μL) sampling loop or preconcentrator injector. The analytes were sampled into the sampling loop or preconcentrator and injected into the μcolumn, with separation conducted under isothermal conditions for single analytes or with corresponding temperature ramping rates for chromatograms (i.e., analyte mixtures). The 5 m μcolumn was used for all in laboratory experiments (i.e., detection limit, linearity, and standard samples), while the 10 m μcolumn was used for practical chromatograms (i.e., breath and car exhaust). Heating was controlled by the integrated

https://doi.org/10.1021/acssensors.1c00482
ACS Sens. 2021, 6, 2348−2355

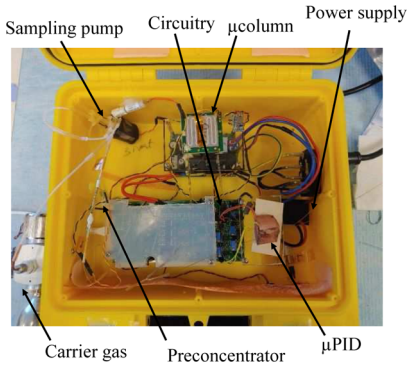

Figure 2. Photograph of the μGC−PID system with components labeled. The system has dimensions 27 × 24 × 10 cm and is entirely self-contained, excluding the computer at signal output.

heater on the column surface. All heating, pumping, and valve switching was controlled via in-house developed LabVIEW software. The only required user input was setting relevant temperature programming parameters and initiating the program; once started, the μGC−PID system could sample and run autonomously. 99.5% purity helium was used as the carrier gas. Finally, considering a carrier gas flow rate of 2 mL/min, the 95 mL (2.4 g of helium) cartridges used were capable of lasting >100 h of operation, more than enough for a day trip in the field.

RESULTS AND DISCUSSION

Detection Limit Characterization. For trace vapor analysis, low limits of detection are required for accurate analysis. The μPID's detection limit was thus characterized on 14 compounds (Tables 1 and S2) and compared to a conventional benchtop FID (Agilent 6890N). Injections on the FID were made using a gas-tight syringe in split mode. Sample separations of hexane and octane with comparison to FID signals are shown in Figure S4. Detection limits were obtained by first calculating the SNR of peaks obtained from injection masses ranging from 100 to 200 pg (except for o-xylene, the injection mass was 432.2 pg). The noise was calculated based on averaging the standard deviation noise (1σ) of ten 3 s-segments of the baseline signal, yielding σ = 0.0162 mV. The detection limits were calculated by dividing injection masses by corresponding SNRs (3σ noise level). Notably, these detection limits were obtained without any preconcentration (i.e., only a 12 cm long 1.875 μL sampling loop was used) in order to examine the μPID's intrinsic performance.

Table 1. μPID Detection Limits of Various VOCs Taken at 3σ, with σ = 0.0162 mV[a]

compound	μPID DL (pg)	FID DL (pg)	IA (pg)	IP (eV)
hexane	0.93	0.73	125.5	10.18
heptane	0.18	0.75	135.4	10.08
octane	0.21	0.84	125.8	9.82
benzene	0.23	0.49	129.0	9.25
toluene	0.19	0.77	173.4	8.82
ethylbenzene	0.26	0.58	116.9	8.77
o-xylene	0.22	0.67	432.2	8.56
ethyl acetate	0.61	0.82	113.4	10.11
butyl acetate	0.24	0.60	127.9	10.01
2-pentanone	0.22	0.39	100.8	9.40
tetrahydrofuran	0.26	0.76	128.7	9.40
isopropanol	0.65	0.64	104.9	10.12
2-butanol	0.24	0.66	117.6	10.10
acetone	0.21	0.40	143.9	9.69

[a]FID detection limits are provided for comparison (σ_{FID} = 0.0059 pA). Detection limits were calculated as averages based on three measurements. Ionization potentials (IPs) and injection amounts (IAs) are also reported for convenience. The μPID had lower detection limits than the FID on all compounds except for hexane and isopropanol. Detection limits using the lowest injection amounts made are also provided in Table S3.

Table 1 shows that the μPID detection limit for many compounds with ionization potentials below ∼10.1 eV is around 0.2−0.3 pg, outperforming the commercial FID that has detection limits around 0.7 pg. The μPID detection limit is increased for compounds with ionization potentials closer to 10.6 eV, such as ethyl acetate, isopropanol, and hexane. As compared to the previously reported μPID (ref 25), the current μPID exhibited a ∼20-fold improvement in the detection limit, which was facilitated by the following factors. First, the VUV illumination area was increased to ∼14 mm^2 from 3.5 mm^2, which is nearly the same as the total area of the VUV lamp window. This allows almost all of the photons emitted from the lamp to be utilized for analyte ionization, especially considering the short illumination path of 400 μm. Additionally, although the distance between the electrodes is increased to 400 μm from 150 μm, the bias voltage was quadrupled to 24 V (corresponding to an electric field of 600 V/cm), allowing for efficient capture of ions in the collection channel; in other words, the ion transit time was maintained to be very short, resulting in high ion collection efficiency. Combined with the low contact resistance, optimized circuit, and component shielding, these parameters resulted in both increased signal strength and decreased noise level, resulting in a sub-picogram detection limit.

Linearity. In Figure 3, μPID linearity was examined for seven compounds with injection masses ranging from as low as 10 pg to 10 ng for each compound. Highly linear responses were observed over the entire range, with a linear dynamic range of at least 5 orders of magnitude observed for all compounds. Notably, the μPID was linear even for low injection amounts around 10 pg, showing that even extremely low injection amounts could be detected by the system. Additional analysis is provided in Table S4, which lists μPID sensitivity and sensitivity normalized by molecular weight.

System Robustness. For a portable system, robustness and stability over device lifetime are important in order to avoid unnecessary maintenance and calibration due to drift. The entire μGC−PID system was run for 3 months without replacement or maintenance of any parts and exhibited no difference in performance at the end of the 3-month period compared to at the start of the period. Analysis on stability was performed by assessing the baseline and noise levels of the μPID readout signal over a 12-week period, as well as examining the system's detection limit on heptane over the μPID run lifetime (Figure 4). The baseline and noise levels demonstrated low variability over the 12-week period, with the baseline level varying from 0.1370 to 0.1372 V, and the noise varying from 0.0138 to 0.0189 mV (average 0.0165 mV), suggesting that system drift over time was minimal. The system was also analyzed over 200 h of μPID operation, in which the plasma was active in order to assess degradation due to plasma etching of the krypton lamp as well as photon bombardment of the microfluidic chip. The system detection limit on heptane showed no significant differences over these 200 h of μPID

https://doi.org/10.1021/acssensors.1c00482
ACS Sens. 2021, 6, 2348−2355

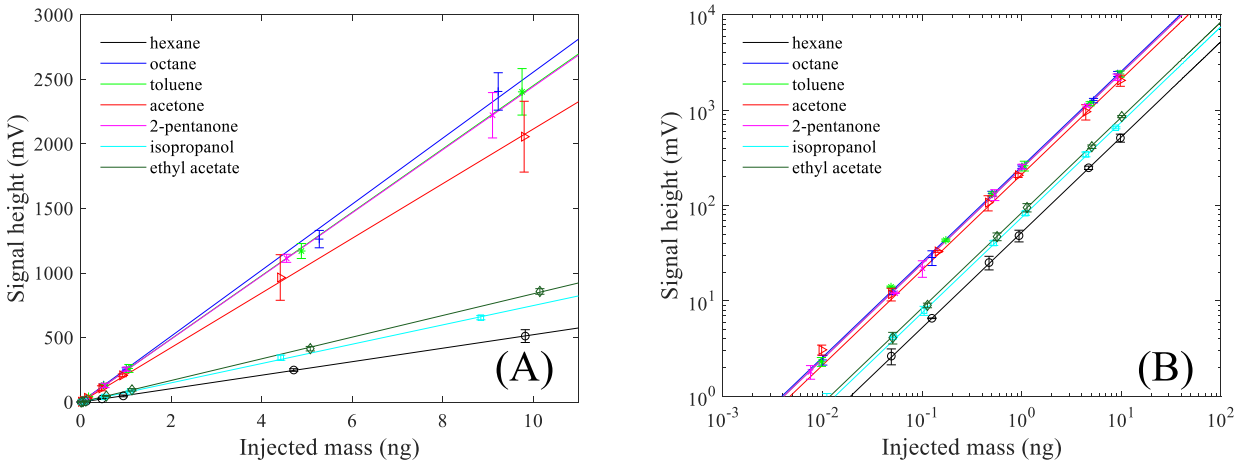

Figure 3. μPID linearity on seven compounds with injection masses ranging from ~10 pg to ~10 ng. (A) Signal heights versus injected masses plotted in a linear−linear scale. (B) Signal heights versus injected masses plotted in a log−log scale. Error bars are obtained from three measurements. The R^2 values for the seven linear fits are 0.9999, 0.9981, 0.9998, 0.9996, 1.0000, 0.9994, and 0.9997 from hexane to ethyl acetate, respectively.

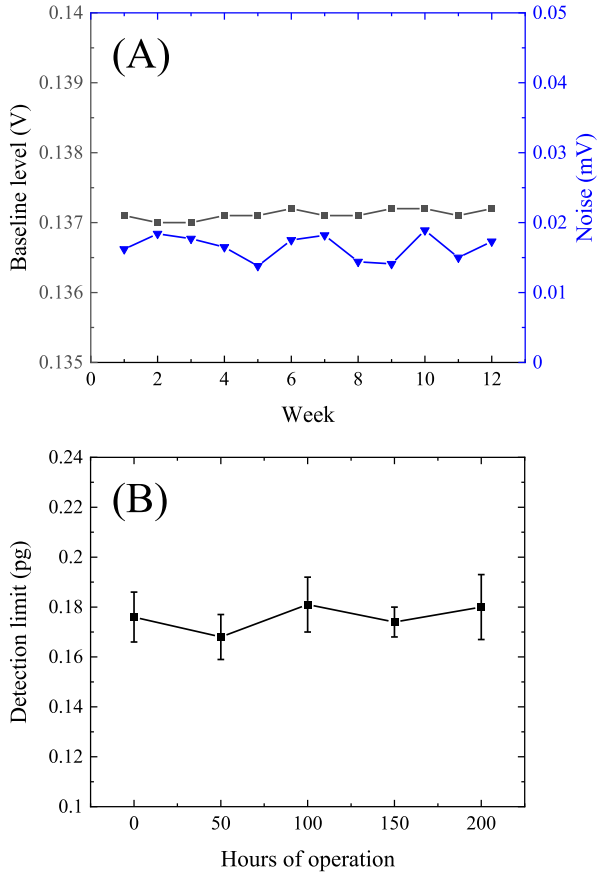

Figure 4. System repeatability. (A) Baseline and noise levels were examined over a 12-week period with low variation over the entire period. Each data point is an average of ten 3 s time samples. (B) μPID detection limit on heptane over 200 h of operation. No significant differences in the detection limit were observed. Data points were calculated from three repeated injections. Error bars represent one standard deviation.

operation, ranging from only 0.168−0.181 pg. This further demonstrates the μGC−PID system's overall stability and capability to run without maintenance or calibration.

GC Standard Chromatograms. The μGC−PID capability for GC separation was examined by analysis of three different standard samples, as shown in Figure 5. Three different samples of alkanes, aromatics, and ketones and acetates were performed at low sample concentrations of around ~3 ng/L (low parts per billion-level concentrations) and sampled using an in-house developed stainless steel preconcentrator. These low concentrations are similar to required levels for trace vapor analysis, such as for indoor air screening. The temperature ramping was controlled by pulse width modulation of the integrated heater, with approximate temperatures given in blue. The carrier gas flow rate was set to 2.1 mL/min. The sampling rate was set to 20 mL/min and the sampling time was 10 min, allowing for clear signals, as shown in Figure 5. Considering the sampling volume of 200 mL, concentration of 3 ng/L, and the SNRs observed in Figure 5, the μGC−PID detection limit can reach as low as 0.14 ppt (by volume) on o-xylene or below ~1 ppt for aromatic compounds, ketones and acetates, and alkanes larger than hexane (Table S5). This single digit to sub-parts per trillion detection limit (in only 200 mL sample volume) is significant improvement over previous sub-parts per billion detection limit systems[20,31,40,43] and is mainly facilitated by the high sensitivity of the μPID.

An additional separation of EPA 502/524.4 VOC mix was performed in Figure 6. The mixture was diluted to approximately ~10 ng/L, sampled at 20 mL/min for 10 min, and injected into the system. For this chromatogram, the flow rate was reduced to 1.2 mL/min, but the temperature ramping was increased to allow for complete separation within only 2 min. Figure 6 demonstrates the μGC−PID system's applicability to environmental analysis, especially trace vapor analysis, due to the PID's high sensitivity. For alternative or more exotic separations such as polar or chiral compounds, other columns such as high-polarity columns or ionic liquid-based[47] columns can be used to replace the OV-1 column used in this system.

Practical Chromatograms. In order to assess the μGC−PID system's capability for *in situ* analysis, practical chromatograms were obtained on breath and car exhaust. For these chromatograms, the 5 m OV-1 μcolumn used in the prior sections was replaced with a 10 m OV-1 μcolumn of the same

https://doi.org/10.1021/acssensors.1c00482
ACS Sens. 2021, 6, 2348−2355

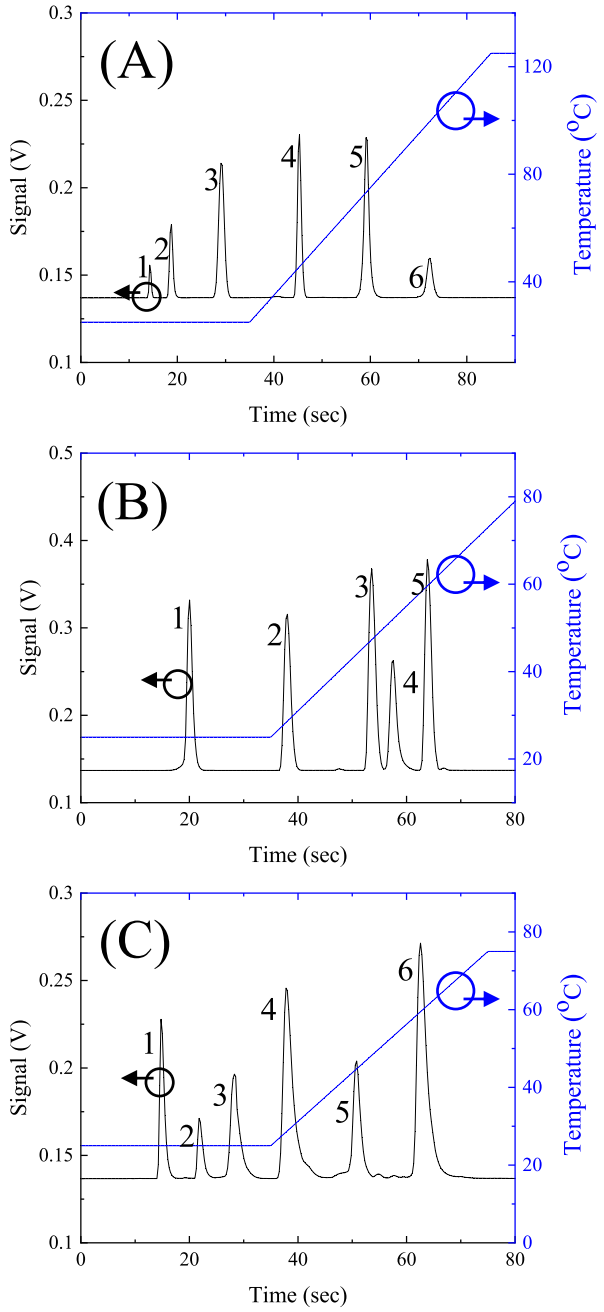

Figure 5. Chromatograms of various sample mixtures (each compound ~3 ng/L) with approximate temperature profiles. The flow rate was 2.1 mL/min. The sampling rate was ~20 mL/min, and the sampling time was 10 min. (A) Alkanes (1) hexane; (2) heptane; (3) octane; (4) nonane; (5) decane; (6) undecane. (B) Aromatics (1) benzene; (2) toluene; (3) ethylbenzene; (4) chlorobenzene; (5) o-xylene. (C) Ketones and acetates (1) acetone; (2) ethyl acetate; (3) methyl isobutyl ketone; (4) butyl acetate; (5) 2-hexanone; (6) 2-heptanone.

stationary phase thickness. Figure 7 shows a chromatogram of human breath sampled from a Tedlar bag at a rate of 20 mL/min for 1 min. The flow rate was set to 2.1 mL/min. C_6 to C_{11} alkane marker retention times are also labeled on the chromatogram for reference. The chromatogram presented in Figure 7 matches closely with previously reported chromatograms in ref 48, demonstrating the capability for rapid

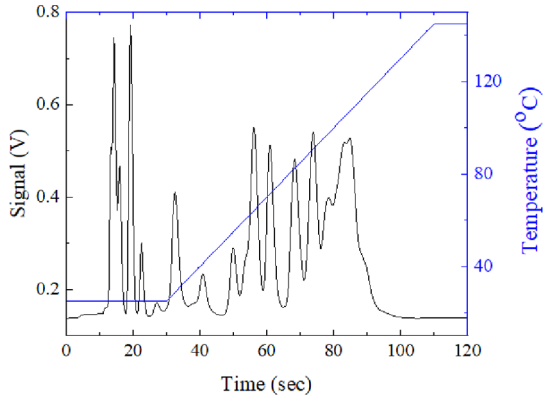

Figure 6. Separation of EPA 502/524 VOC mix (each component ~10 ng/L). The flow rate was 1.2 mL/min. The sampling rate was ~20 mL/min, and the sampling time was 10 min. The entire separation time was less than 2 min.

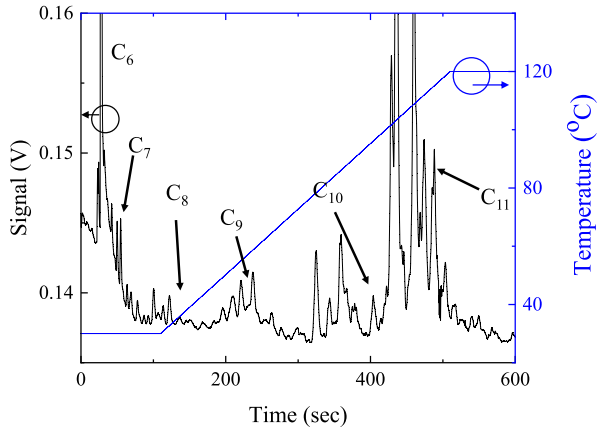

Figure 7. Separation of human breath. The flow rate was 2.1 mL/min. The sampling rate was ~20 mL/min, and the sampling time was 1 min. Retention times of C_6–C_{11} alkane markers are provided for reference.

separation and detection of a complex practical sample with minimal sampling time.

An additional separation of car exhaust was performed by sampling pure car exhaust from a Hyundai Accent 2019 at a rate of 20 mL/min for 1 min. The carrier gas flow rate was again set to 2.1 mL/min, resulting in the chromatogram shown in Figure 8. Benzene, toluene, ethylbenzene, and xylene (BTEX) marker retention times are labeled on the chromatogram for reference. The peak height in Figure 8 tends to increase near the BTEX markers, which are commonly and expectedly found in most car exhausts. This suggests that this μGC–PID system could be used for toxic vapor analysis in areas with large quantities of motor vehicle emissions, such as near highways or in large cities. Overall, these chromatograms demonstrate the capability of this system for practical analysis of vapor samples outside of the lab.

CONCLUSIONS

The development of a highly sensitive μPID with sub-picogram detection limit and large dynamic range for a wide range of VOCs has been detailed herein, demonstrating comparable or better detection limit compared to benchtop FID. This device was used to construct a completely automated μGC–PID system (including miniaturized preconcentrator and micro-

https://doi.org/10.1021/acssensors.1c00482
ACS Sens. 2021, 6, 2348–2355

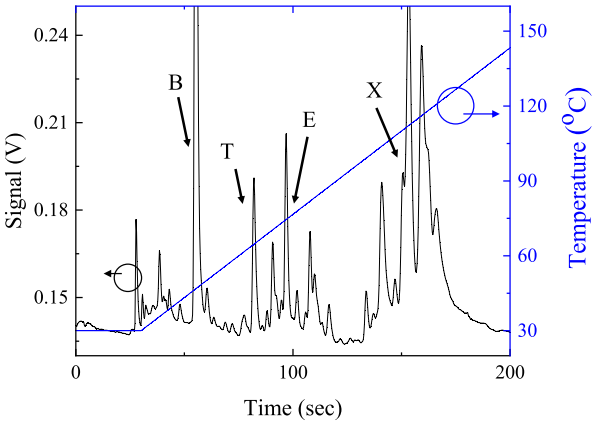

Figure 8. Separation of car exhaust. The flow rate was 2.1 mL/min. The sampling rate was ~20 mL/min, and the sampling time was 1 min. Retention times of aromatic markers are provided for reference. B: benzene; T: toluene; E: ethylbenzene; X: xylene.

fabricated column along with μPID) capable of detecting sub-parts per trillion concentrations of VOCs in a 200 mL sample volume, enabling rapid *in situ* trace VOC analysis. Future work may target further lowering the μPID detection limit by an additional 10-fold to tens of fg, which may involve increasing the VUV light intensity and illumination area, as well as increasing the bias electric field. This would allow for development of an ultra-sensitive μGC−PID with the detection limit rivaling that of benchtop mass spectrometry equipped with an electron multiplier tube.

■ ASSOCIATED CONTENT

Supporting Information

The Supporting Information is available free of charge at https://pubs.acs.org/doi/10.1021/acssensors.1c00482.

High-sensitivity μGC−PID for trace vapor detection, supplemental system assembly and fabrication processes, and additional performance analysis (PDF)

■ AUTHOR INFORMATION

Corresponding Author

Xudong Fan − *Department of Biomedical Engineering, University of Michigan, Ann Arbor, Michigan 48109, United States; Center for Wireless Integrated MicroSensing and Systems (WIMS²), University of Michigan, Ann Arbor, Michigan 48109, United States;* orcid.org/0000-0003-0149-1326; Email: xsfan@umich.edu

Authors

Maxwell Wei-Hao Li − *Department of Biomedical Engineering and Department of Electrical Engineering and Computer Science, University of Michigan, Ann Arbor, Michigan 48109, United States; Center for Wireless Integrated MicroSensing and Systems (WIMS²), University of Michigan, Ann Arbor, Michigan 48109, United States*

Abhishek Ghosh − *Department of Biomedical Engineering, University of Michigan, Ann Arbor, Michigan 48109, United States; Center for Wireless Integrated MicroSensing and Systems (WIMS²), University of Michigan, Ann Arbor, Michigan 48109, United States*

Anandram Venkatasubramanian − *Department of Biomedical Engineering, University of Michigan, Ann Arbor, Michigan 48109, United States; Center for Wireless Integrated MicroSensing and Systems (WIMS²), University of Michigan, Ann Arbor, Michigan 48109, United States*

Ruchi Sharma − *Department of Biomedical Engineering, University of Michigan, Ann Arbor, Michigan 48109, United States; Center for Wireless Integrated MicroSensing and Systems (WIMS²), University of Michigan, Ann Arbor, Michigan 48109, United States*

Xiaolu Huang − *Department of Biomedical Engineering, University of Michigan, Ann Arbor, Michigan 48109, United States; Center for Wireless Integrated MicroSensing and Systems (WIMS²), University of Michigan, Ann Arbor, Michigan 48109, United States*

Complete contact information is available at: https://pubs.acs.org/10.1021/acssensors.1c00482

Author Contributions

‖M.W.-H.L and A.G. have equal contribution to the paper.

Notes

The authors declare the following competing financial interest(s): The micro-ionization detector technology used in the article is licensed to Nanova. X.F. is a co-inventor of this technology and he also serves as a paid consultant to Nanova.

■ ACKNOWLEDGMENTS

The authors acknowledge the support from National Institute for Occupational Safety and Health (NIOSH) via R01 OH011082-01A1 and from the Office of the Director of National Intelligence (ODNI), Intelligence Advanced Research Projects Activity (IARPA), via IARPA FA8650-19-C-9101. The views and conclusions contained herein are those of the authors and should not be interpreted as necessarily representing the official policies or endorsements, either expressed or implied, of the ODNI, IARPA, or the U.S. Government. The U.S. Government is authorized to reproduce and distribute reprints for Governmental purposes notwithstanding any copyright annotation thereon. The authors acknowledge microfabrication aid from the Lurie Nanofabrication Facility at the University of Michigan.

■ REFERENCES

(1) Grate, J. W. Acoustic wave microsensor arrays for vapor sensing. *Chem. Rev.* **2000**, *100*, 2627−2648.

(2) Kauffman, D. R.; Star, A. Carbon nanotube gas and vapor sensors. *Angew. Chem., Int. Ed. Engl.* **2008**, *47*, 6550−6570.

(3) Albert, K. J.; Lewis, N. S.; Schauer, C. L.; Sotzing, G. A.; Stitzel, S. E.; Vaid, T. P.; Walt, D. R. Cross-reactive chemical sensor arrays. *Chem. Rev.* **2000**, *100*, 2595−2626.

(4) Szulczyński, B.; Gębicki, J. Currently Commercially Available Chemical Sensors Employed for Detection of Volatile Organic Compounds in Outdoor and Indoor Air. *Environments* **2017**, *4*, 21.

(5) Mirzaei, A.; Leonardi, S. G.; Neri, G. Detection of hazardous volatile organic compounds (VOCs) by metal oxide nanostructures-based gas sensors: A review. *Ceram. Int.* **2016**, *42*, 15119−15141.

(6) Cho, B.; Lee, K.; Jo, E.; Kim, J. Detection of Mixed BTEX With Suppressed Reaction Specificity Using Tin Oxide Nanoparticles Functionalized by Multi-Metalloporphyrins. *IEEE Sens. J.* **2019**, *19*, 11791−11796.

(7) Singh, E.; Meyyappan, M.; Nalwa, H. S. Flexible Graphene-Based Wearable Gas and Chemical Sensors. *ACS Appl. Mater. Interfaces* **2017**, *9*, 34544−34586.

(8) Wales, D. J.; Grand, J.; Ting, V. P.; Burke, R. D.; Edler, K. J.; Bowen, C. R.; Mintova, S.; Burrows, A. D. Gas sensing using porous materials for automotive applications. *Chem. Soc. Rev.* **2015**, *44*, 4290−4321.

(9) Bai, H.; Shi, G. Gas sensors based on conducting polymers. *Sensors* **2007**, *7*, 267−307.
(10) Sun, Y.-F.; Liu, S.-B.; Meng, F.-L.; Liu, J.-Y.; Jin, Z.; Kong, L.-T.; Liu, J.-H. Metal oxide nanostructures and their gas sensing properties: a review. *Sensors* **2012**, *12*, 2610−2631.
(11) Zhou, X.; Lee, S.; Xu, Z.; Yoon, J. Recent Progress on the Development of Chemosensors for Gases. *Chem. Rev.* **2015**, *115*, 7944−8000.
(12) Mirzaei, A.; Kim, J.-H.; Kim, H. W.; Kim, S. S. Resistive-based gas sensors for detection of benzene, toluene and xylene (BTX) gases: a review. *J. Mater. Chem. C* **2018**, *6*, 4342−4370.
(13) Spinelle, L.; Gerboles, M.; Kok, G.; Persijn, S.; Sauerwald, T. Review of Portable and Low-Cost Sensors for the Ambient Air Monitoring of Benzene and Other Volatile Organic Compounds. *Sensors* **2017**, *17*, 1520.
(14) Patel, S. V.; Hobson, S. T.; Cemalovic, S.; Mlsna, T. E. Chemicapacitive microsensors for detection of explosives and TICs. *Proc. SPIE* **2005**, *5986*, 59860M.
(15) Qin, Y.; Gianchandani, Y. B. A fully electronic microfabricated gas chromatograph with complementary capacitive detectors for indoor pollutants. *Microsyst. Nanoeng.* **2016**, *2*, 15049.
(16) Hobbs, P. J.; Misselbrook, T. H.; Pain, B. F. Assessment of Odors from Livestock Wastes by a Photoionization Detector, an Electronic Nose, Olfactometry and Gas-Chromatography Mass-Spectrometry. *J. Agric. Eng. Res.* **1995**, *60*, 137−144.
(17) Rezende, G. C.; Le Calvé, S.; Brandner, J. J.; Newport, D. Characterization of a modular microfluidic photoionization detector. *Sens. Actuators, B* **2020**, *324*, 128667.
(18) Skog, K. M.; Xiong, F.; Kawashima, H.; Doyle, E.; Soto, R.; Gentner, D. R. Compact, Automated, Inexpensive, and Field-Deployable Vacuum-Outlet Gas Chromatograph for Trace-Concentration Gas-Phase Organic Compounds. *Anal. Chem.* **2019**, *91*, 1318−1327.
(19) Price, J. G. W.; Fenimore, D. C.; Simmonds, P. G.; Zlatkis, A. Design and operation of a photoionization detector for gas chromatography. *Anal. Chem.* **2002**, *40*, 541−547.
(20) Zhou, Q.; Zhang, S.; Zhang, X.; Ma, X.; Zhou, W. Development of a Novel Micro Photoionization Detector for Rapid Volatile Organic Compounds Measurement. *Appl. Bionics Biomechanics* **2018**, *2018*, 1.
(21) Driscoll, J. N. Evaluation of a New Photoionization Detector for Organic-Compounds. *J. Chromatogr.* **1977**, *134*, 49−55.
(22) Soo, J.-C.; Lee, E. G.; LeBouf, R. F.; Kashon, M. L.; Chisholm, W.; Harper, M. Evaluation of a portable gas chromatograph with photoionization detector under variations of VOC concentration, temperature, and relative humidity. *J. Occup. Environ. Hyg.* **2018**, *15*, 351−360.
(23) Zhang, W.-q.; Li, H.; Zhang, Y.-j.; Bi, F.; Meng, L.-s.; Zhang, X.-m.; Mao, J.-y.; Cheng, N.-l.; Fang, B.; Yang, Y.; Chen, C.; Guo, K.-x.; Zhan, G.-e.; Sha, J.; Wang, X.-z. Fast Determination of Monocyclic Aromatic Hydrocarbons in Ambient Air Using a Portable Gas Chromatography−Photoionization Detector. *Chromatographia* **2017**, *80*, 1233−1247.
(24) Jia, M.; Koziel, J.; Pawliszyn, J. Fast field sampling/sample preparation and quantification of volatile organic compounds in indoor air by solid-phase microextraction and portable gas chromatography. *Field Anal. Chem. Technol.* **2000**, *4*, 73−84.
(25) Zhu, H.; Nidetz, R.; Zhou, M.; Lee, J.; Buggaveeti, S.; Kurabayashi, K.; Fan, X. Flow-through microfluidic photoionization detectors for rapid and highly sensitive vapor detection. *Lab Chip* **2015**, *15*, 3021−3029.
(26) Lee, J.; Zhou, M.; Zhu, H.; Nidetz, R.; Kurabayashi, K.; Fan, X. Fully Automated Portable Comprehensive 2-Dimensional Gas Chromatography Device. *Anal. Chem.* **2016**, *88*, 10266−10274.
(27) Zrodnikov, Y.; Rajapakse, M. Y.; Peirano, D. J.; Aksenov, A. A.; Kenyon, N. J.; Davis, C. E. High Asymmetric Longitudinal Field Ion Mobility Spectrometry Device for Low Power Mobile Chemical Separation and Detection. *Anal. Chem.* **2019**, *91*, 5523−5529.
(28) Sun, J.; Guan, F.; Cui, D.; Chen, X.; Zhang, L.; Chen, J. An improved photoionization detector with a micro gas chromatography column for portable rapid gas chromatography system. *Sens. Actuators, B* **2013**, *188*, 513−518.
(29) Lee, J.; Zhou, M.; Zhu, H.; Nidetz, R.; Kurabayashi, K.; Fan, X. In situ calibration of micro-photoionization detectors in a multi-dimensional micro-gas chromatography system. *Analyst* **2016**, *141*, 4100−4107.
(30) Poole, C. F. Ionization-based detectors for gas chromatography. *J. Chromatogr. A* **2015**, *1421*, 137−153.
(31) Pang, X.; Nan, H.; Zhong, J.; Ye, D.; Shaw, M. D.; Lewis, A. C. Low-cost photoionization sensors as detectors in GCxGC systems designed for ambient VOC measurements. *Sci. Total Environ.* **2019**, *664*, 771−779.
(32) Rezende, G.; Le Calvé, S.; Brandner, J.; Newport, D. Micro Milled Microfluidic Photoionization Detector for Volatile Organic Compounds. *Micromachines* **2019**, *10*, 228−239.
(33) Rezende, G. C.; Le Calvé, S.; Brandner, J. J.; Newport, D. Micro photoionization detectors. *Sens. Actuators, B* **2019**, *287*, 86−94.
(34) Narayanan, S.; Rice, G.; Agah, M. A micro-discharge photoionization detector for micro-gas chromatography. *Microchim. Acta* **2013**, *181*, 493−499.
(35) Lewis, A. C.; Hamilton, J. F.; Rhodes, C. N.; Halliday, J.; Bartle, K. D.; Homewood, P.; Grenfell, R. J. P.; Goody, B.; Harling, A. M.; Brewer, P.; Vargha, G.; Milton, M. J. T. Microfabricated planar glass gas chromatography with photoionization detection. *J. Chromatogr. A* **2010**, *1217*, 768−774.
(36) Li, J.; Hodges, R. D.; Gutierrez-Osuna, R.; Luckey, G.; Crowell, J.; Schiffman, S. S.; Nagle, H. T. Odor Assessment of Automobile Cabin Air With Field Asymmetric Ion Mobility Spectrometry and Photoionization Detection. *IEEE Sens. J.* **2016**, *16*, 409−417.
(37) Verner, P. Photoionization detection and its application in gas chromatography. *J. Chromatogr. A* **1984**, *300*, 249−264.
(38) Driscoll, J. N.; Duffy, M. Photoionization detector: A versatile tool for environmental analysis. *Chromatography* **1987**, *2*, 21−27.
(39) Freedman, A. N. The photoionization detector: Theory, performance and application as a low-level monitor of oil vapour. *J. Chromatogr. A* **1980**, *190*, 263−273.
(40) You, D.-W.; Seon, Y.-S.; Jang, Y.; Bang, J.; Oh, J.-S.; Jung, K.-W. A portable gas chromatograph for real-time monitoring of aromatic volatile organic compounds in air samples. *J. Chromatogr. A* **2020**, *1625*, 461267.
(41) Bocos-Bintintan, V.; Smolenschi, A.; Ratiu, I. A. Rapid Determination of Indoor Air Contaminants in Shoe Shops Using Photoionization Detectors. *Stud. Univ. Babes-Bolyai, Chem.* **2016**, *61*, 203−212.
(42) Pyo, S.; Lee, K.; Noh, T.; Jo, E.; Kim, J. Sensitivity enhancement in photoionization detector using microelectrodes with integrated 1D nanostructures. *Sens. Actuators, B* **2019**, *288*, 618−624.
(43) Lara-Lbeas, I.; Rodríguez-Cuevas, A.; Andrikopoulou, C.; Person, V.; Baldas, L.; Colin, S.; Le Calvé, S. Sub-ppb Level Detection of BTEX Gaseous Mixtures with a Compact Prototype GC Equipped with a Preconcentration Unit. *Micromachines* **2019**, *10*, 187−199.
(44) Akbar, M.; Shakeel, H.; Agah, M. GC-on-chip: integrated column and photoionization detector. *Lab Chip* **2015**, *15*, 1748−1758.
(45) Narayanan, S.; Rice, G.; Agah, M. Characterization of a micro-helium discharge detector for gas chromatography. *Sens. Actuators, B* **2015**, *206*, 190−197.
(46) Li, M. W.-H.; Ghosh, A.; Sharma, R.; Zhu, H.; Fan, X. Integrated microfluidic helium discharge photoionization detectors. *Sens. Actuators, B* **2021**, *332*, 129504.
(47) Li, M. W.-H.; Huang, X.; Zhu, H.; Kurabayashi, K.; Fan, X. Microfabricated ionic liquid column for separations in dry air. *J. Chromatogr. A* **2020**, *1620*, 461002.
(48) Zhou, M.; Sharma, R.; Zhu, H.; Li, Z.; Li, J.; Wang, S.; Bisco, E.; Massey, J.; Pennington, A.; Sjoding, M.; Dickson, R. P.; Park, P.; Hyzy, R.; Napolitano, L.; Gillies, C. E.; Ward, K. R.; Fan, X. Rapid breath analysis for acute respiratory distress syndrome diagnostics

https://doi.org/10.1021/acssensors.1c00482
ACS Sens. 2021, 6, 2348−2355

using a portable two-dimensional gas chromatography device. *Anal. Bioanal. Chem.* **2019**, *411*, 6435−6447.

https://doi.org/10.1021/acssensors.1c00482
ACS Sens. 2021, 6, 2348−2355